Regional Gravity Survey of Silver Spurs Ranch

Wes Wilson

Sangre Geophysics

November 2, 2006

Disclaimer:

Opinions expressed are solely those of the author and do not reflect those of the Silver Spurs Property Owners Association.

Motivation

The geology of the Spanish Peaks is unique. Emplacement of the Spanish Peaks created a series of radial faults which allowed the formation of dikes that permeate the region.

Many ground water systems are fracture controlled. Dikes and associated fracture patterns create a complex water flow regime where groundwater flow is redirected by impermeable dikes. By understanding large scale fractures and subsurface dike locations, connected regions of water flow can begin to be identified.

The purpose of this study is to establish whether or not the Spanish Peak dikes extend into Silver Spurs Ranch, and if so where are they and at what depth. Results are evaluated to determine possible connected water flow regions and possible areas of recharge where the water flow is replenished.

A geophysical gravity survey provides a relatively inexpensive subsurface mapping tool for large regional areas. This report presents the results of a geophysical survey conducted over the Silver Spurs Ranch in June, 2006.

Regional geology

The surface geology of the Spanish Peaks area has been strongly influenced by the formation of the Spanish Peaks. The Spanish Peaks are thought to be large intruded magma bodies called stocks or batholiths. These bodies formed at depth some 27 million years ago and gradually became visible as the softer overlying rock eroded away.

When the Spanish Peak stocks were formed, vertical forces of the hot rock caused fractures to form in the overlying sedimentary rocks. As the fractures were created, hot magma flowed into the cracks to form the dikes. Figure 1 shows an outcrop of a typical dike just north of the town of La Veta. Typical widths of the dikes range from a few meters to tens of meters.

Simple mathematical models based on point stresses in thin plates predict expected fracture patterns to be radial arcs. The arcs curve at the ends to align with existing horizontal stress in the plate. Figure 2 shows the Spanish Peaks as seen from a point of view above Silver Spurs Ranch looking west. Major dikes are outlined in blue to emphasize their radial nature. Not all dikes follow the same radial pattern. This suggests that the dikes most likely formed over a period time under different stress conditions.

Horizontal and vertical stresses associated with the dikes also left a vertical fault imprint in the weaker overlying sedimentary layers. Figure 3 shows vertical factures in the Trinidad sandstone formation, a rock layer found beneath Silver Spurs Ranch.

Dikes and vertical fracturing control water flow through out the region. The ability of water to flow through rock is measured as permeability. Permeability of the dike rock is higher than the surrounding sedimentary rock. When water flow encounters a buried dike it is diverted along the vertical plane of the dike. Water flowing in sedimentary rocks will seek out channels provided by existing vertical fractures. The combination of dikes and fractures create a complex water flow pattern in the region. By understanding the location of the dikes both above and below the surface, water barriers created by dikes can be outlined to understand water flow patterns.

The physical properties of the dike rock that create higher permeability also make the rock heavier or denser. Surrounding sedimentary rock is less dense than the dike rock. A gravity survey takes advantage of the density contrast to map the location of the subsurface dikes.

Gravity survey design

A gravity survey measures the pull of gravity at various survey locations. The pull of gravity varies as a function of rock density. Gravity differences on the surface of the earth are small but measurable. Refer to Appendix C for a detailed description of the gravity exploration method as presented by the United States Geological Survey (USGS).

A gravity survey is one of the most inexpensive geophysical techniques for mapping the subsurface. The survey is conducted by taking a series of measurements over the survey area. A regional gravity survey was conducted on Silver Spurs Ranch over the period June 16 - 20, 2006. Gravity measurements were taken along existing roads at a spacing of 100 meters (m). This resulted in 368 measurements along 36.8 linear kilometers (23 miles). The survey covered approximately 31 square kilometers (12 square miles). Measurement locations are shown with respect to the Spanish Peaks in Figure 4.

To determine density contrast, rock samples were taken from several locations on Silver Spurs Ranch (The Ranch). Densities for rock sample locations shown in Figure 4 are listed in Table 1. Samples WAL1 and WAL2 are taken from a dike outcrop along Highway 85 north of Walsenburg. They indicate an average dike density of 3.85 grams per cubic centimeter (g/cc).

site	rock type	density g/cc
WAL1	hornblende	4.09
WAL2	hornblende	3.60
SSP1	sandstone	2.36
SSP2	sandstone	2.37
SSP3	sandstone	2.63
SSP4	sandstone	2.37

Table 1 Rock sample density measurements.

The average density of the 4 sandstone samples is 2.43 g/cc. A density difference of 1.42 g/cc between the sandstone and dike rocks is large enough to create a change in gravity that can be measured by an exploration gravity meter.

Gravity surface locations are displayed on a USGS topographical map in Figure 5. Universal Transversal Mecator (UTM) coordinates are annotated along the map axes. Gravity station (stn) locations and the corresponding UTM coordinates (XYs) are listed in Appendix B.

Roads on the USGS maps are taken from an older vintage aerial photo and the road locations vary from their present day locations as shown by gravity survey markers along current roads. For reference, the property map, Figure 6, will be shown with the gravity maps. The property map is shown with a digital elevation map in Figure 7.

Gravity measurement

At each survey location a gravity measurement is made along with latitude, longitude and elevation. Layout for a typical gravity measurement is shown in Figure 8. The gravity meter is about the size of a car battery and is shown with the aluminum carrying case. The carrying case contains a battery which powers the temperature control and readout displays. The top view of the gravity meter shows the controls, Figure 9. A measurement is made by first setting the meter on a tripod base. The instrument is leveled using the large knobs on the left side corners and middle right.

Once level, the aluminum dial is rotated until the 'beam' galvanometer in the upper right reads zero or is straight up. Gravity values are then read off the aluminum dial.

Once the gravity value is read, the latitude, longitude and elevation are read from the Garmin GPS receiver shown at the upper left in Figure 8. The latitude/longitude GPS coordinates were read to within an accuracy of about 10-20 meters. Vertical measurements of elevation were accurate to 20m at best. For a gravity survey, accurate vertical elevation measurements are critical for determining gravity corrections. To improve vertical accuracy, the latitude/longitude locations for each measurement were used to locate the corresponding elevation on the USGS map in Figure 5. The Garmin GPS receiver and the USGS map use the WGS84 projection. Elevations (elev) in meters for each location are listed in Appendix B.

Measurements are noted in the black survey book, the meter is locked and set into the aluminum carrying case, equipment is loaded into the truck and the next survey location is found by driving along the road 100m using the GPS receiver for reference. Each measurement took from 4-8 minutes.

A cross section of the gravity meter is shown in Figure 10. The gravity meter contains a sensitive spring which balances an internal mass on a beam. The mass is balanced by turning the nulling dial which corresponds with the aluminum dial shown in Figure 9. The gravity meter used for the survey was a Lacoste and Romberg D meter with a sensitivity of about .1 mgal gravity units. For reference, the surface gravity along the equator of the earth is about 1 million mgal. The gravity meter measures to less than 1 part per million of the total gravity field.

Gravity corrections

A number of factors influence a gravity measurement. When the gravity survey is corrected for known variations, the resulting gravity map shows the unknown or anomalous gravity. Gravity anomalies are modeled mathematically based on known density variations to determine possible subsurface bodies or, in this case, dike locations.

Gravity measurements are affected by the following known factors:

- Electronic instrument drift during the course of the survey
- Tidal variation caused by the sun and moon
- Latitude variations caused by the shape of the earth
- Elevation differences along the survey profile
- Density difference beneath a corrected datum elevation
- Elevation differences in the surrounding terrain

Electronic instrument drift occurs in any electronic instrument. Instrument heating, stray capacitance and other factors cause a measuring device to change slightly over time. The gravity meter is no exception. To correct for instrument drift, base stations are established during the survey as reference points. A base station measurement is made, several gravity station measurements are made and then the base station is re-measured to identify any instrument drift. For this survey, a base station was re-measured every 2 hours at a maximum. Instrument drift is assumed to be linear between stations and is removed from the measurements. Details of each correction are summarized in Appendix A.

Tidal pull of the sun and moon also affect the gravity measurement. Tidal corrections can be computed mathematically, but in general the variation is assumed to be linear over the time frame of the drift correction. The correction is applied at the same time as the drift correction. Appendix B shows the actual field reading from the gravity meter, 'field g', in gravity meter units. The 'rel g' column shows the relative gravity value in mgal units with the drift corrections applied. The survey base station was established on the SE corner of the driveway at 463 Leather Dr. To find absolute

gravity measurements the ‘rel g’ value is added to a known gravity station established by the US Geodetic Survey. Such a station exists at Trinidad Junior College and a measurement was made for completeness of the survey. However, when looking for anomalies, only the change in gravity is needed. Therefore, relative gravity changes are used for interpretation.

Gravity is caused by presence of mass. Any object with mass has a gravitational attraction. As one moves away from the mass, the gravitational attraction decreases. The same is true for the earth. As one moves away from the earth, the gravitational attraction decreases. The earth is not completely solid and as the earth turns, the centrifugal force causes the earth to bulge along the equator. The bulge causes the surface of the earth to be farther away from the center of the earth at the equator than at the poles. This causes the measured gravity to be lower at the equator than at the poles. The change is a function of the shape of the earth, and the shape is well known from satellite measurements. The correction is known as a latitude correction formally defined as the International Association of Geodesy Reference System 1980. Gravity measurements with the applied latitude correction are listed in the column marked ‘latitude’ in Appendix B.

Elevation change causes a change in gravity. An elevation profile along Silver Spurs Rd from north to south, Figure 11, shows an elevation variation of approximately 170m. For an average density of 2.67 g/cc, this elevation difference results in a gravity change of 50 mgals. Since the dike anomalies are less than 10 mgals, an elevation correction must be made to the field measurements. The correction is called a free air correction. The ‘free air’ column in Appendix B shows the gravity measurements which have been corrected for drift, latitude and elevation. These measurements are referenced to a constant elevation datum of 2076 m, the elevation of the base station.

The free air gravity values are contoured to generate a free air anomaly map, Figure 13. The anomaly map is shown with the digital elevation map in Figure 12. Color contours are in gravity units of mgal shown annotated on the color bar. The free air anomaly map generally follows the topography. Figure 12 shows gravity highs in red roughly following the elevation highs along the ridges found on The Ranch.

Two additional corrections are necessary before attempting an interpretation, the Bouguer correction and the terrain correction. The free air correction compensates for elevation variations with reference to a datum elevation. The Bouguer correction adjusts the gravity measurements to fill in the surface below the datum and removes the surface above the datum. The resulting gravity measurement is as if it was measured on a flat surface at the datum elevation. The Bouguer correction is combined with the free air correction to generate the ‘bouger’ values in Appendix B. The corresponding Bouguer anomaly map is seen in Figures 14 and 15.

The Bouguer anomaly map highlights regions of excess mass. A large positive anomaly of 3 mgal is seen around properties 39 and 40 along Silver Spur Rd. Although large, it is smaller than the free air anomaly of 11 mgals at the same location. There does not appear to be a direct correlation of the anomalies with the topography. This suggests that a gravity correction related to the surrounding terrain may be necessary.

The complete Bouguer anomaly map, Figures 16 and 17, takes into account terrain corrections about each gravity measurement. Appendix B lists the anomaly values in the column marked ‘complete.’ The complete Bouguer anomaly map shows a general correlation with topography as expected and will form the basis of the gravity interpretation.

Gravity modeling

The complete Bouguer anomaly map shows remaining gravity variations after all corrections are made. Anomalies associated with the near subsurface geology are interpreted by matching a computed gravity field above blocky models to the observed gravity anomaly. When the field

matches, one possible solution has been determined. The technique is referred to interchangeably as either 'modeling' or 'interpretation.'

The gravity field for simple geometric structures like rectangles and n-sided polygons can be computed for a given density. To simplify the gravity modeling, the subsurface can be assumed to be 2 dimensional (2D). This assumption gives a good approximation when the 2D cross section is taken perpendicular to the trend of the gravity anomaly. A 3D approximation is made by assuming that the 2D model continues into and out of the plane. This is called a 2.5D approximation. To visualize, one can consider a loaf of bread. The slice of bread in the center of the loaf would be the 2D model and the entire loaf of bread would be the 2.5D model.

Gravity modeling was accomplished with Geomodel, a modeling software package. The program allows a user to interactively define 2.5D geometric blocks to match the observed gravity anomaly. Block vertices can be adjusted interactively to refine the interpretation.

The complete Bouguer anomaly map with 6 selected 2.5D profiles lines is shown in Figure 18. Four of the lines are taken along the trend of the gravity anomalies and two are taken perpendicular. Gravity values are extracted along these profiles and block models are created to match the gravity changes.

Profile AA' , Figure 19, is a 2D cross section which starts near the end of Rope Ct and trends northeast to Reins Rd. The starred (*) points represent gravity values in mgals which have been extracted form the complete Bouguer map along the AA' profile. The solid line is the gravity computed for the model blocks shown in green. Depth and horizontal axis units are meters.

The object of gravity modeling is to match the computed gravity anomaly with the observed gravity values. The resulting model reflects the depth and extent of dike structures.

A constant density is required for computing the gravity field. Values shown on the green blocks represent density contrast values between the dike rock and the surrounding sandstone. Referring to Table 1 for measured density values, a value of 1.5 was chosen to represent the density contrast. This value was used for all density blocks for consistency. Surface positions and lateral extent of the density blocks are shown in Figure 25.

The topographic map, Figure 16, suggests that ridges to the west of the survey may extend into the The Ranch. Body 1 on Profile AA' indicates a dike extending along the trend of the ridge possibly extending the length of Profile AA'. Body 2 is a cross cutting dike. It shows up again in Profile BB' and extends the length of Rowell Rd to Sunset Ct. Body 3 required a long lateral extent to match the gravity anomaly. The lateral extent may indicate a possible influence from the large gravity anomaly related to Body 4. A dike outcrop in the creek bed along Silver Spur Rd indicates that the dike associated with Body 3 most likely trends to the northwest. Body 4 has a large associated gravity anomaly and may either be an extension of the dike from the south or an extension from a dike trending west to east outside The Ranch or both. Depths to the top of the dikes vary from 80-90m for dikes 1 and 2 along the south side to depths of 140-200m along Reins Rd to the north. Figure 26 shows a possible interpretation of the cross cutting dike structure.

Profile BB', Figure 20, starts along Silver Spur Rd to the north and runs SSE to the south end of The Ranch. As mentioned, Body 1 most likely extends along Rowell Rd to Sunset Ct and possibly beyond. Body 2 is a broad gravity anomaly that ranges across The Ranch to at least Sunrise Rd. A short lateral extent was used for the density block. The computed gravity anomaly was relatively insensitive to lateral extent because of the required depth of the perturbing blocks. The dike appears to start around Boot Ct and extends to Sunrise Rd. Body 3 indicates a cross cutting dike structure that trends west to east along Horseshoe Ct and Leather Dr. The anomaly is discussed in detail for Profile EE'. Similarly, Body 4 shows the intersection of Profile BB' with the Small Dike anomaly along Profile FF'. Depths to top of the anomalies range from 110-140m for the narrow

cross cutting dikes, Bodies 3 and 4, to a relatively deep 325m for the broad anomaly associated with Body 2.

Profile CC', Figure 21, follows Sunrise Rd and intersects Small Dike to the south. Body 1 may be a small dike following the west to east trend shared with the major dike features. Body 2 is an extension of the broad gravity anomaly seen along Profile BB'. The gravity anomaly appears smeared and may indicate 3D effects from nearby features. Profile DD' along the ridge of the broad dike feature shows a break in the anomaly at the intersection with Profile BB'. The break may indicate a fault which strikes NNE and will be discussed in more detail when profiles DD' and EE' are evaluated. Body 3 represents the intersection with Small Dike to the south. Bodies 1 and 3 are at depths of 200 m and 180 m respectively. Body 2 is modeled at a depth of 300 m and may reflect a discontinuity along the west to east anomaly modeled in Profile DD'.

Profile DD', Figure 22, starts on the west at Boot Ct, traverses across Silver Spur Rd to Sunrise Rd and ends along Trails End Dr to the east. The gravity anomaly is wide and may indicate a contribution from a second dike within the anomaly. A single polygon is used to model the gravity anomaly since the profile traverses along the ridge of the anomaly. The anomaly begins abruptly around the start of Boot Ct. Profile DD' shows the top of dike gently dipping to the east, starting at a depth of 315m and dropping to a depth of 1700m. A small anomaly along Rodeo Dr, brings the depth back to 30m near the surface. The depth plunges to 4000m and then returns to 250m beneath Trails End Dr. The large depth variation may indicate the dike is offset by a fault. Further evidence for a fault can be found along Profile EE'. The interpretation of the dike and fault are shown in Figure 26.

Profile EE', Figure 23, starts along Horseshoe Circle to the west and travels along Leather Dr down to the old Hezron Mine. The top of the interpreted dike varies from 200-300m along the profile until about property 107 where the interpreted dike drops to a depth of 2000m then returns to a depth of 400m along the Hezron mine ridge. The drop along the top of the surface of the model is interpreted as a fault in Figure 26.

Profile FF', Figure 24, starts along Green Horn View Lane, travels along Silver Spur Rd following Small Dike and ends along Cherokee Lane to the east. The top of the model drops to a depth of 1500m where it first intersects Silver Spur Rd. This may indicate a fault or a smaller cross cutting dike feature. The model returns to a depth of 140m before dropping again to 1500m. This second drop is interpreted as an extension of the fault along Sunrise Rd and Leather Drive. The model returns to a depth of 220m along Cherokee Lane.

Profiles BB' and CC' extend into what appears to be a broad, isolated basin between Small Dike and Big Dike on the south end of The Ranch. A small gravity high occurs in the basin around property 134, but the basin is featureless for the most part. Small gravity changes do not necessarily translate into small topography changes. A surface elevation change of 70m along Pryor Canyon is seen in the same area.

Water Regions

Dikes form impermeable boundaries to water flow. Knowing the position of the dikes, possible water flow regions can be inferred. Figure 27 shows five possible recharge regions associated with the interpreted dike positions. Recharge areas are marked with blue arrows. Any changes to recharge regions in the blue arrow areas may impact well performance in the associated regions on The Ranch.

Region I in the northwest corner of The Ranch was not included in the gravity survey but from the topographic expression of dikes to the west, it is reasonable to assume that water recharge occurs along the dike to the immediate south and is replenished with any available water resource coming from the northwest. The recharge area is marked with blue arrow 1.

Region II at the north end of the Ranch receives recharge water from the south side of the dike to the immediate west. The recharge area is marked with blue arrow 2. The interpreted dike along Reins Rd may redirect the recharge coming from the west causing shadow zones on the east side of the dike. An alternate recharge region to the northeast is marked with blue arrow 4.

Region III in the center of The Ranch has a possible recharge area occurring along Walsen Creek. The digital elevation map, Figure 27, shows a large fault offsetting Big Dike along the Walsen Creek as indicated with blue arrow 3. The fault offset creates a gap of 100m allowing water recharge to flow off the slopes of East Spanish Peak and enter the Region III water regime from the south. The interpreted dike which begins along Chaps Ct and extends along Rowell Rd to Sunrise Ct may discourage recharge from entering Region II from this recharge source. Small Dike bounds Region IIi on the south. Seasonal recharge occurs along the flanks of Small Dike. Along the northeast margin of Region III recharge marked as blue arrow 4 may occur from the plains to the northeast.

Region IV at the south end of The Ranch is isolated from the other recharge zones by Small Dike and Big Dike. The gravity survey indicates that the region is an isolated basin. Figure 5 shows Pryor Canyon beginning along the west edge of Small Dike. Surface runoff travels down Pryor Canyon seeping into fractures along the surface and recharging water resources at depth. A similar type of recharge mechanism occurs along the north side of Big Dike. Water recharge marked as blue arrow 5 may also occur on the southeast margin.

Depths to the top of dike structures are greater than 100m in most areas on The Ranch. This means deep water flow is influenced by dike positions, but near the surface water flow is controlled by existing fractures. Figure 3 shows vertical fractures occurring in the Trinidad sandstone. Similar fractures most likely exist in the Raton sandstone that covers most of The Ranch.

Summary

Gravity surveys are a relatively inexpensive geophysical method which can be used to infer simple subsurface features. The intruded dike complex which permeates Silver Spur Ranch provides a density contrast signature which is measurable. The impermeable dikes impact water flow in region. By knowing the location of subsurface dikes, possible water flow regions are inferred.

The final interpretation, Figure 26, shows dike and fault positions interpreted from the gravity survey. Long linear ridges to the west are consistent with interpreted dikes on The Ranch. Dike ridges tend to lose their distinct appearance once they cross Walsen Arroyo into the Ranch. The gravity survey confirms that the dikes extend into The Ranch at depth.

The gravity anomaly along Reins Rd may represent an extension of a dike from the south west. A dike outcrop in Walsen Arroyo supports this interpretation. The small SSW to NNE trending anomaly which starts at Chaps Ct, crosses Cantrell Rd and continues along Reins Rd, does not correlate well with the predominate dike orientations in the area. However, a dike outcrop along Silver Spur Rd is consistent with the interpretation.

Southwest to northeast trending gravity anomalies correlate well with dikes to the west. Big Dike and Small Dike show positive gravity anomalies. There are 3 smaller east-west trends which indicate buried dikes with depths that range from a hundred meters to thousands of meters.

Along Sunrise Rd the interpreted east-west dike structures drops to thousands of feet. This is interpreted as a possible fault which offsets the dike. A large drop in interpreted depth to the top of the structure along Leather Dr and Silver Spurs Rd to south may be an extension of the same fault.

The region south of Small Dike and north of Big Dike on the south end of The Ranch is relatively free of gravity anomalies. This indicates a large basin with water recharge coming from the bounding Big Dike and Small Dike ridges.

Water regions are defined based on dike locations, Figure 27. There at least four separate water regions with corresponding recharge areas. Dikes permeate the subsurface at depths of more the 100m. This means the dikes control water flow at depth, but near the surface water is controlled by fractures in the overburden.

Future Studies

The gravity survey successfully delineated the general structure of the subsurface dikes. These dikes are a controlling influence on water flow at depth. Above the dikes, water flow is controlled by fractures in the sedimentary rock. Fractures most likely follow the vertical fracture patterns created during the emplacement of the dikes.

For water wells, it is important to know if and where there are fluid filled fractures. One geophysical method that is sensitive to vertical water filled fractures is a method called resistivity. Resistivity surveys measure the electrical conductivity of the earth. A small electrical current is applied to the earth through a pair of electrodes. Another pair of electrodes is used to measure the variation in the electrical field away from the source electrodes. The small current created by 4 D size batteries is non-destructive and does not harm vegetation or structures. A useful study would be to determine the sensitivity of this type of survey in the area.

A near surface seismic survey is more expensive but gives more detail about near surface layers and fracturing. Seismic surveys use a shotgun source which is shot into the ground to generate sound waves. Sound waves are reflected at rock layer boundaries or faults and return to the surface. An array of accelerometers is set on the surface of the earth to record the returning sound waves. Records are processed to create seismic sections which show rock interfaces at depth. The sections outline in detail the existing fracture patterns, but do not guarantee water filled fractures.

Finally, the most accurate measure of the subsurface comes from well data. This is the only direct measurements of the subsurface. Well monitoring will establish seasonal norms for existing wells. A sharp drop or increase from the norm indicates a change in water recharge patterns or water supply. A useful study would be to establish monitoring wells which can be measured monthly. To give a good measurement of static water levels, the monitor well should not be one that is currently being pumped.

Figure 1 Radial dike outcrop along Highway of Legends north of La Veta.

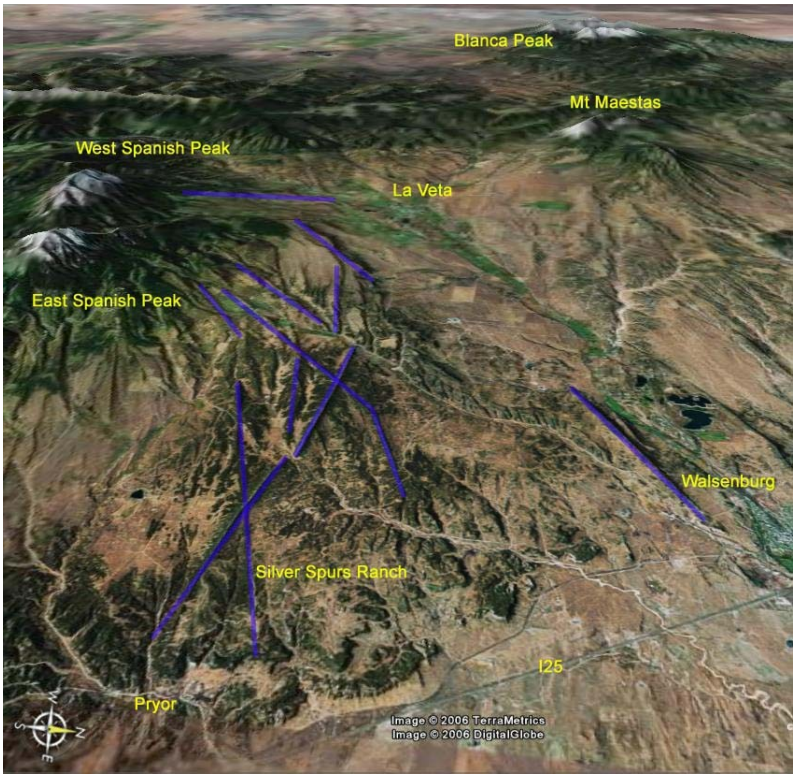

Figure 2 Aerial photo of Spanish Peaks looking west from Silver Spurs Ranch. Major radial dike locations are outlined in blue.

Figure 3 Vertical fractures in the Trinidad sandstone found along County Rd 330 between The Ranch and Walsenburg.

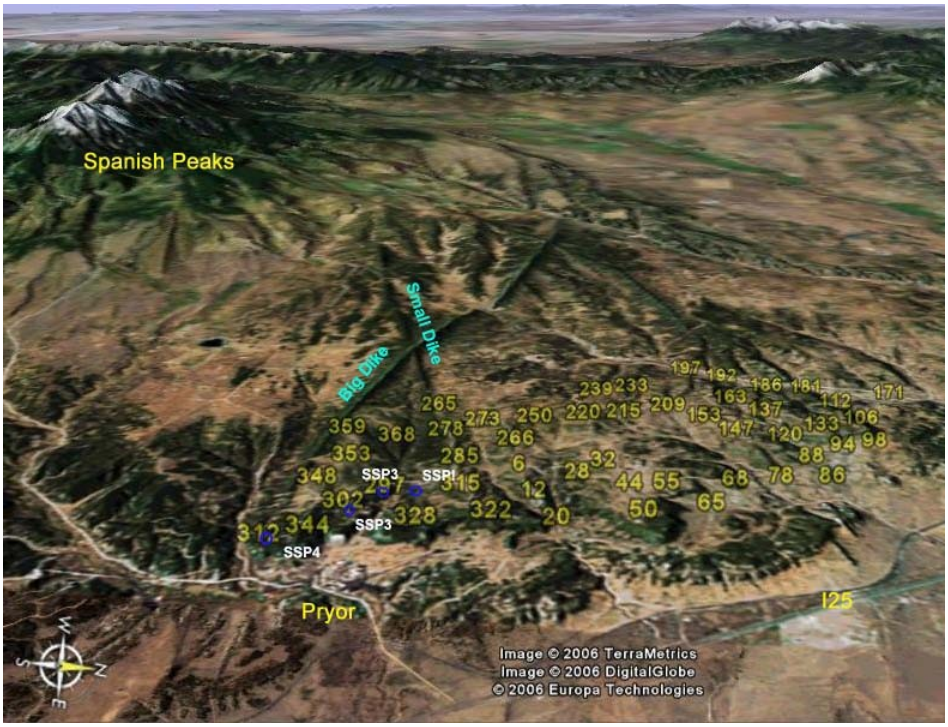

Figure 4 Gravity station locations in yellow and rock sample locations in white. Big Dike and Small Dike can be seen extending into The Ranch.

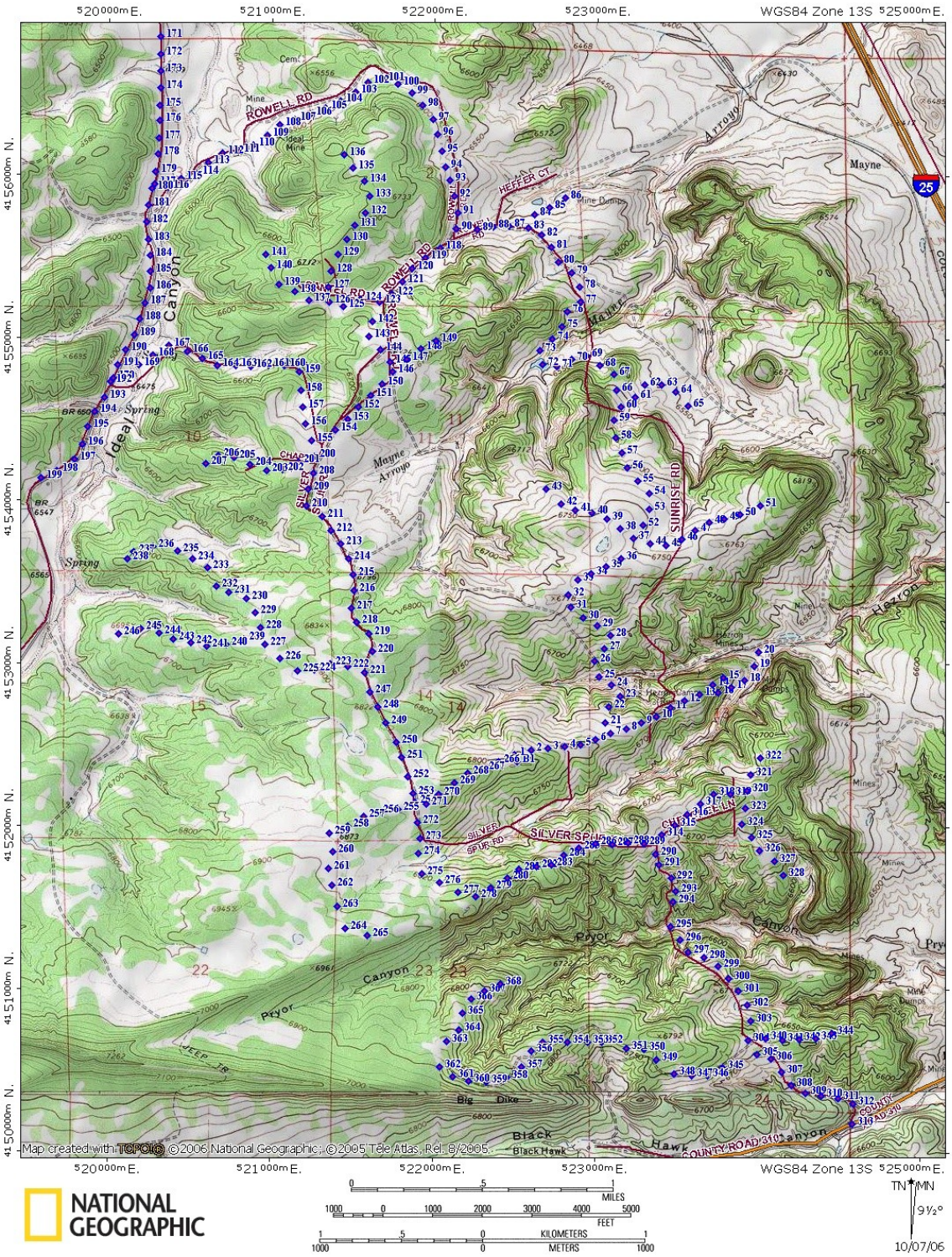

Figure 5 USGS topographic map showing gravity station locations in blue. Road locations appear as they were in the early '90s. Gravity station locations indicate position of current roads.

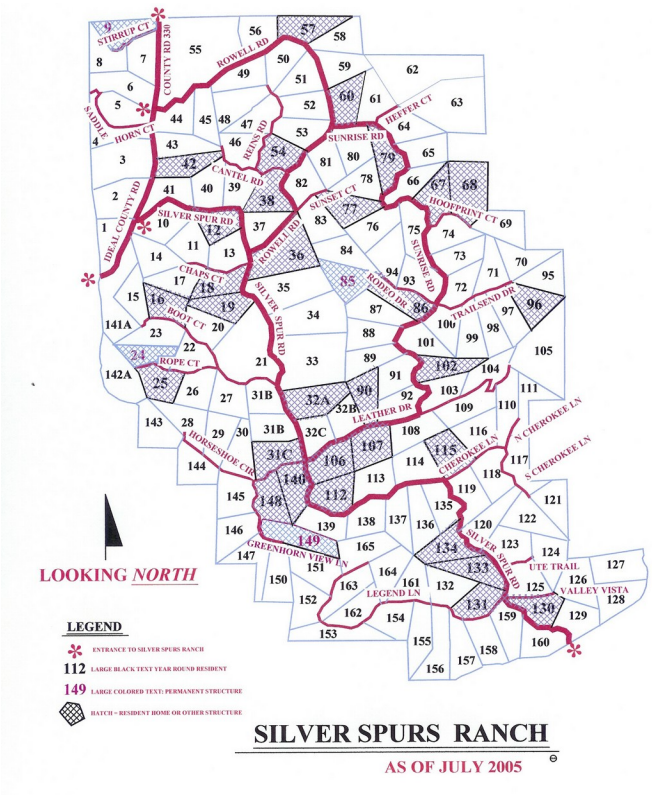

Figure 6 Silver Spurs Ranch property map as of July 2005. The map is used for reference on the gravity anomaly maps.

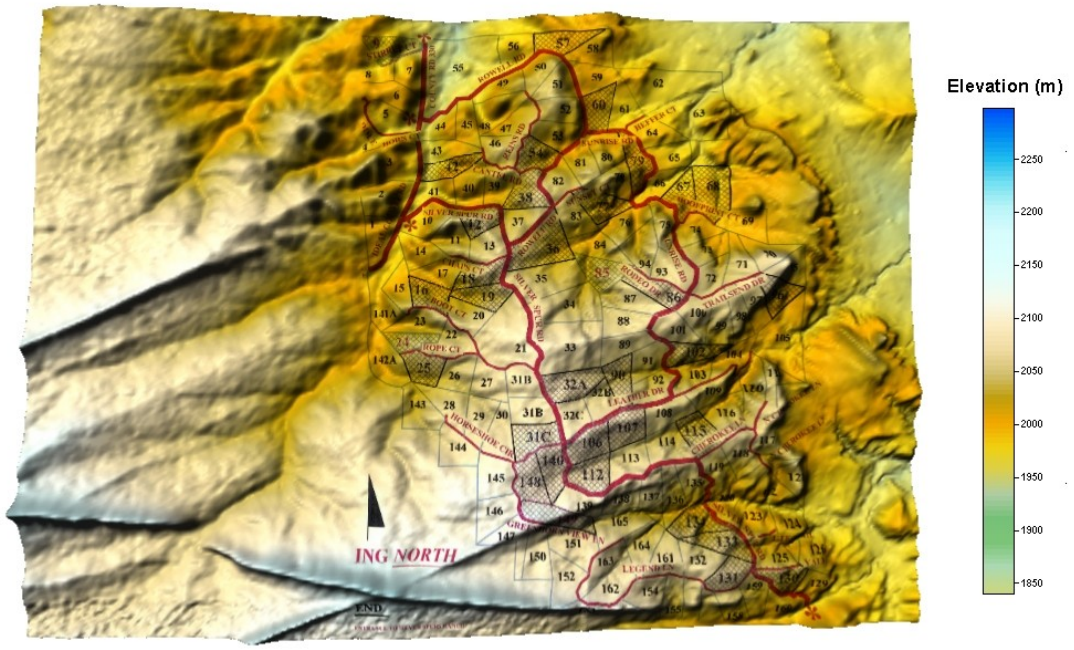

Figure 7 Mosaic of digital elevation maps for the area with property map.

Figure 8 Typical gravity station measurement showing the gravity meter, GPS receiver and field notebook. The towel is for an old man's knees.

Figure 9 Top view of LaCoste and Romberg D gravity meter. Tilt adjustment knobs are located on the left and middle right. Galvonometer dial is above the eyepiece and the aluminum read out dial is in the middle.

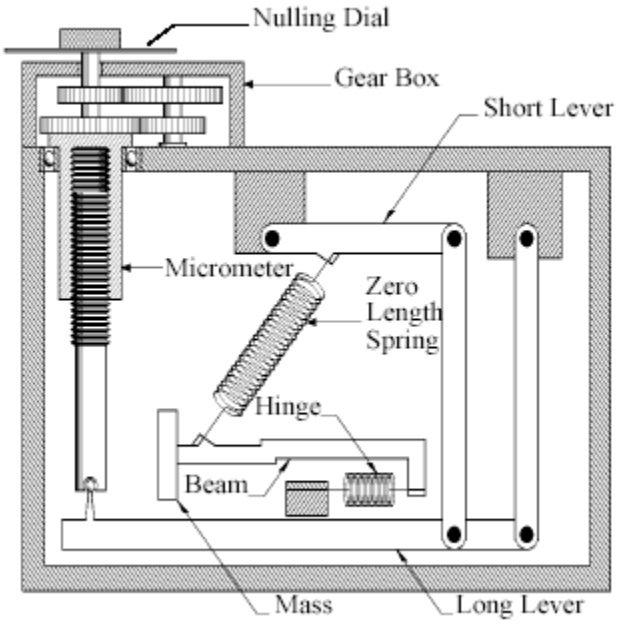

Figure 10 Schematic showing a cross section of the gravity meter. The ultra sensitive Zero Length Spring balances the Mass on the balance Beam. The galvanometer 'beam' measures the Long Lever location with respect to zero.

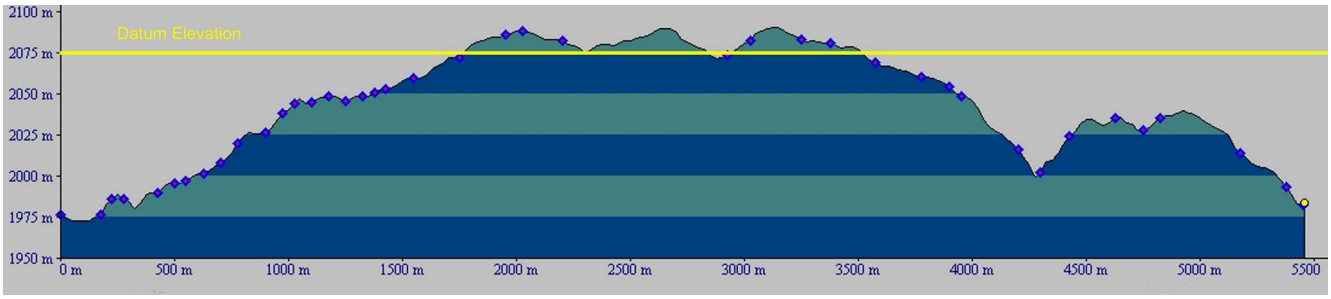

Figure 11 Elevation profile along Silver Spur Rd starting at the mail boxes on the County Rd 330 and ending at the south entrance. Yellow line shows gravity datum elevation at 2076m. Vertical exaggeration is a factor of 12.

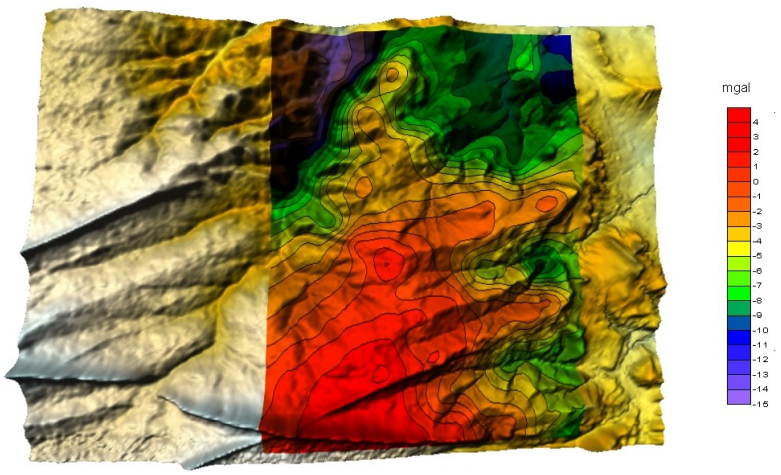

Figure 12 Free air anomaly map shown with regional topography. Red gravity anomaly contours trend along surface ridges.

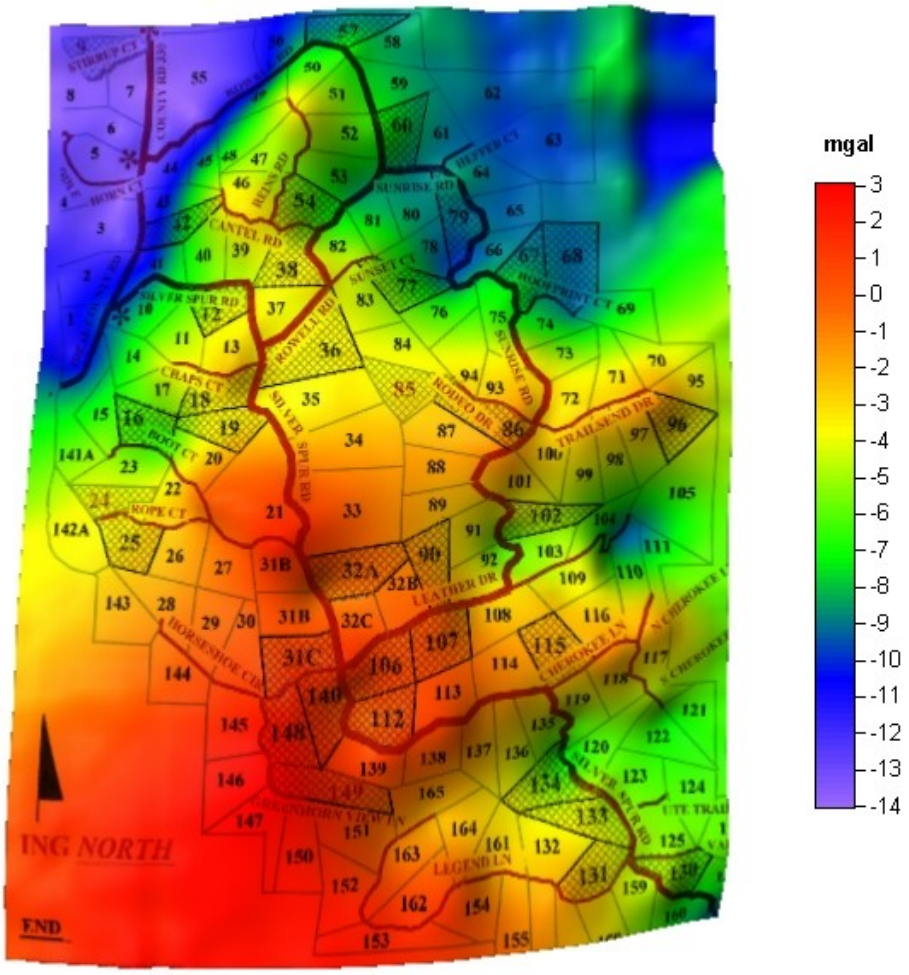

Figure 13 Free air anomaly map shown with property map.

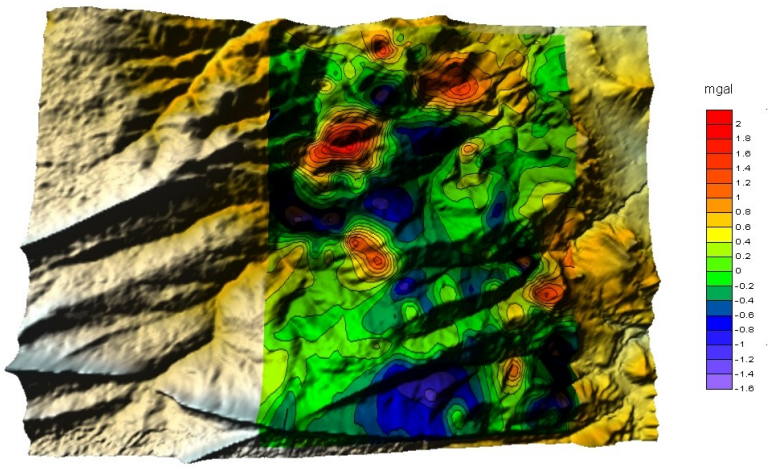

Figure 14 Bouguer anomaly map shown with regional topography.

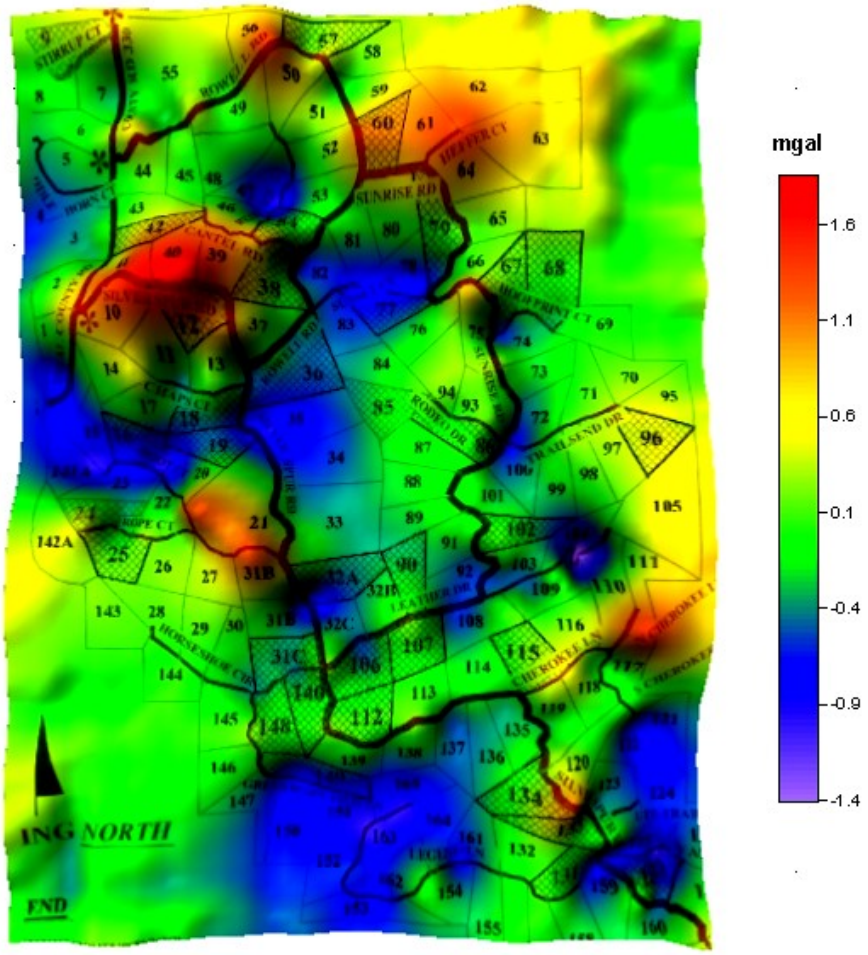

Figure 15 Bouguer anomaly map with property map.

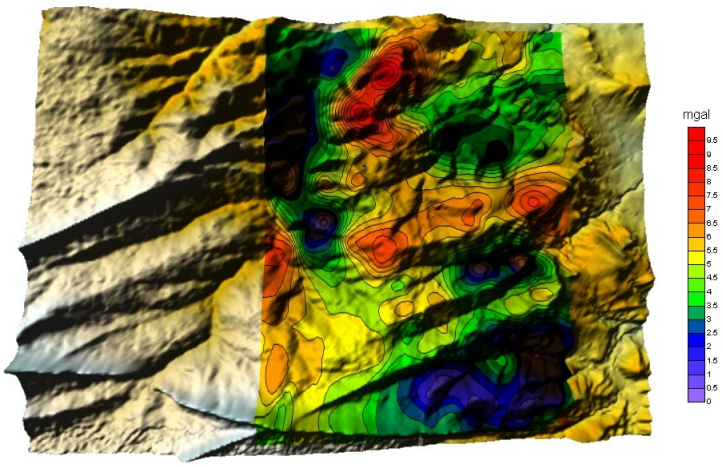

Figure 16 Complete Bouguer anomaly map shown with regional topography.

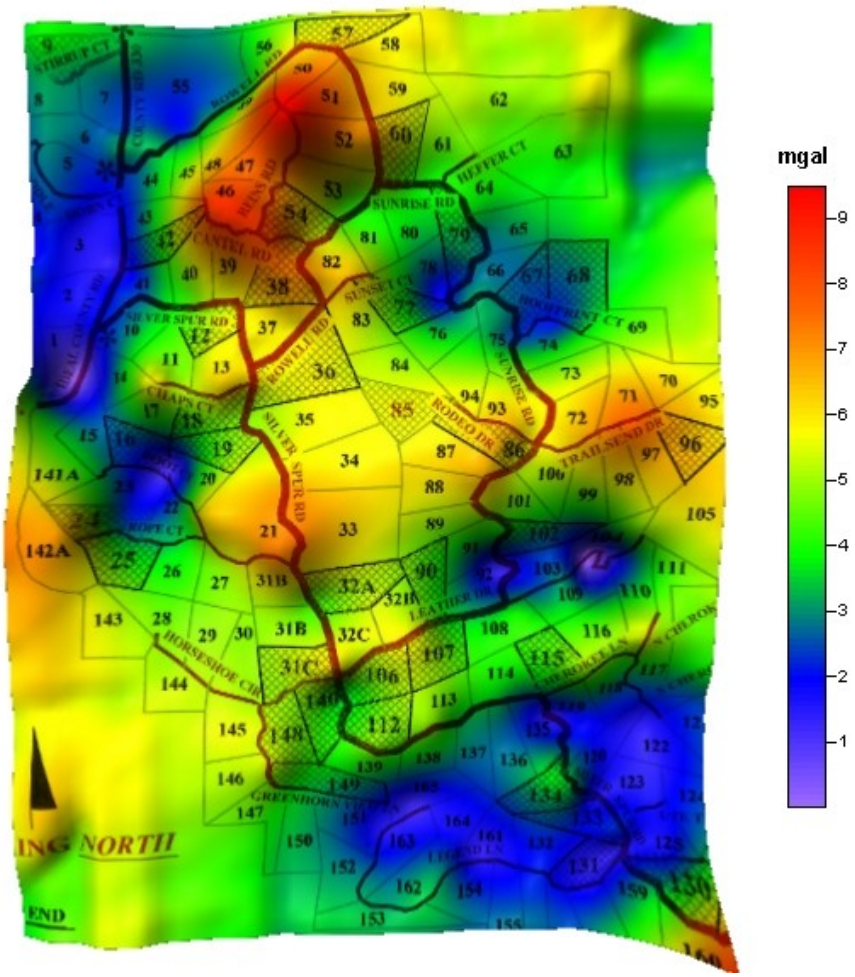

Figure 17 Complete Bouguer anomaly map with property map.

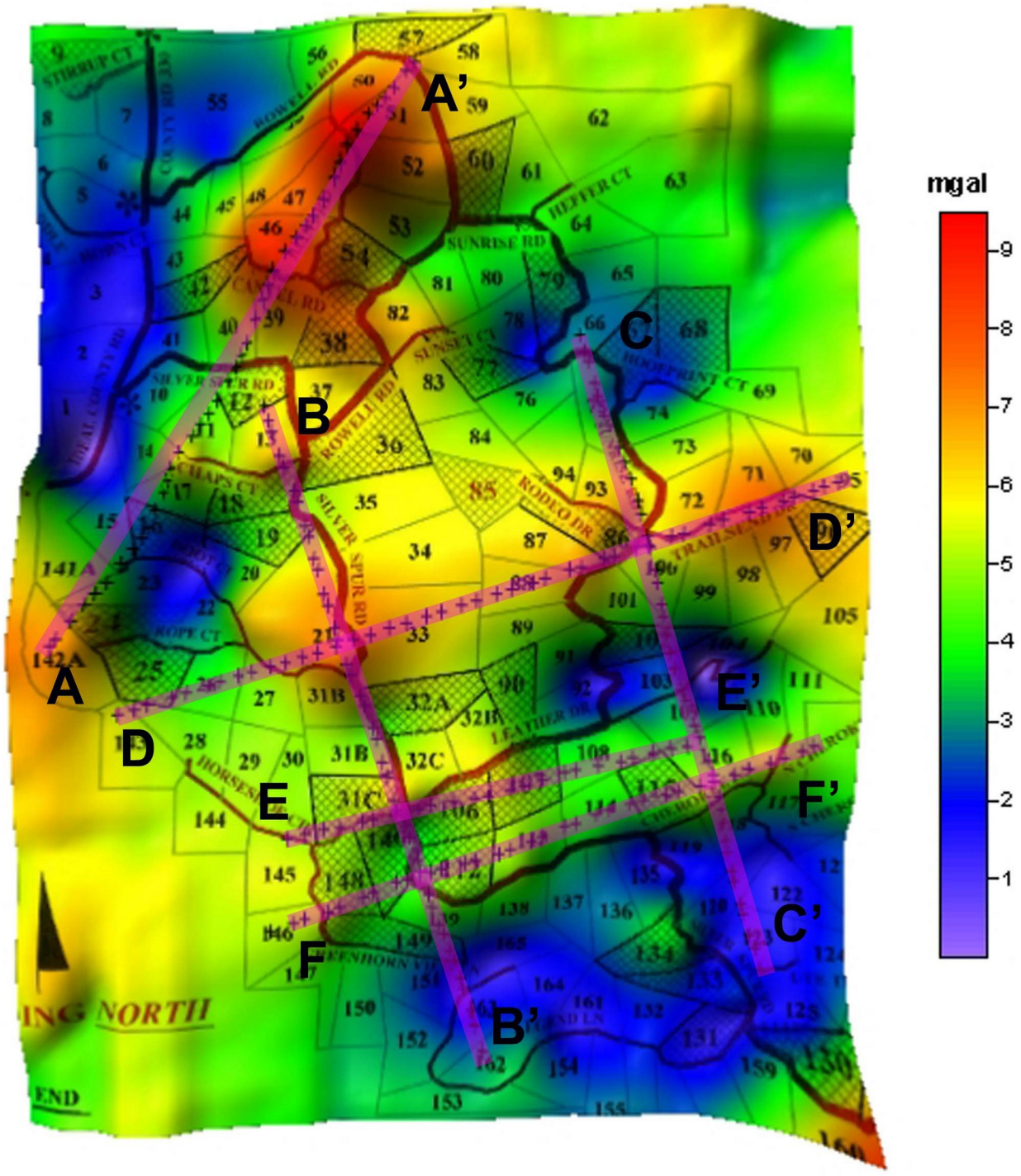

Figure 18 Complete Bouguer anomaly map with gravity modeling profiles.

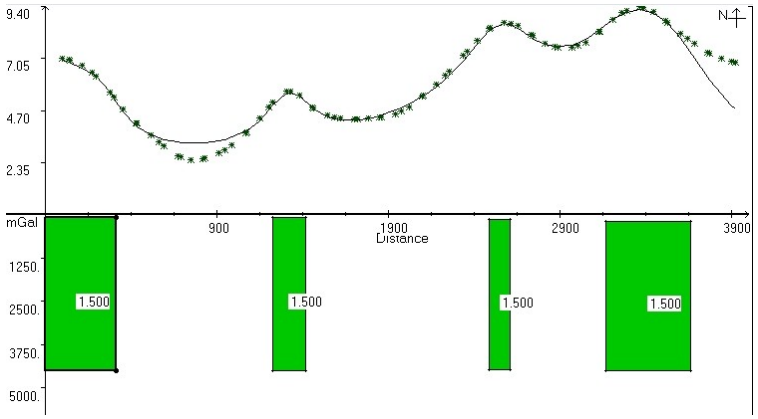

Figure 19 Profile AA', Rope Ct to Reins Rd.

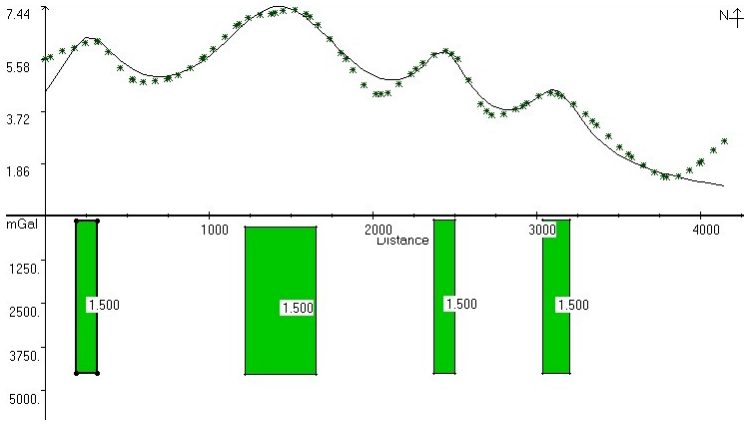

Figure 20 Profile BB', north end of Silver Spurs Rd.

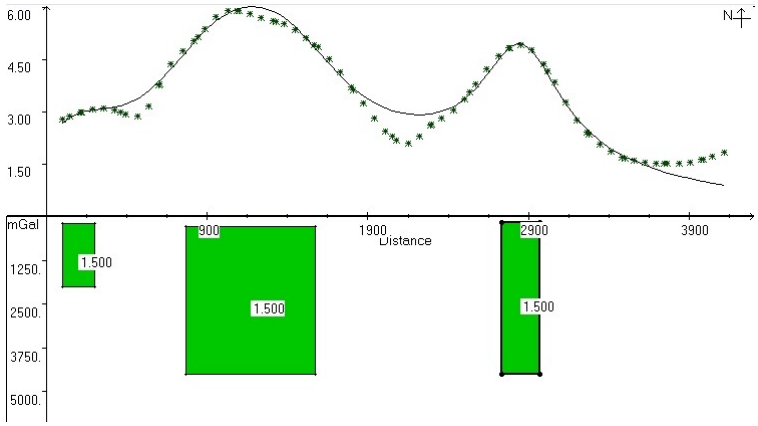

Figure 21 Profile CC', Sunrise Rd to south Silver Spurs Rd.

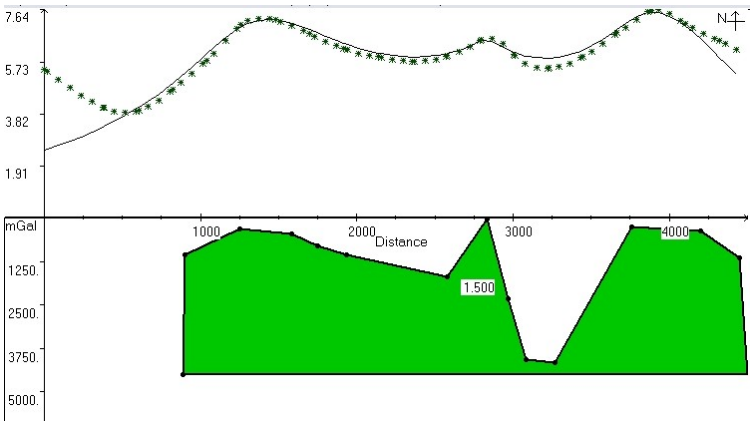

Figure 22 Profile DD', Rope Ct to Trails End Dr.

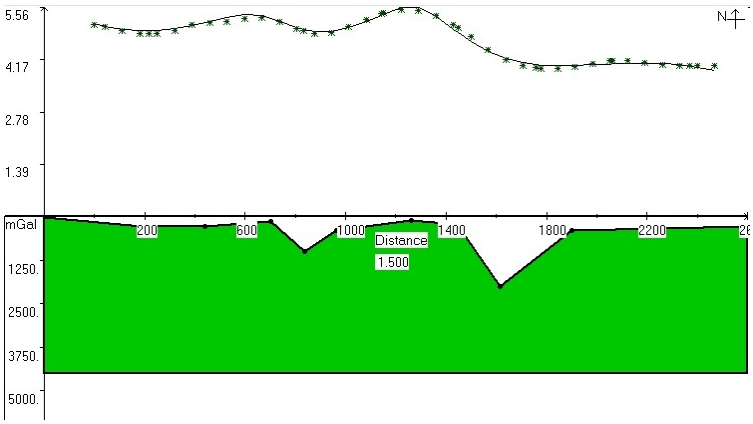

Figure 23 Profile EE', Horseshoe Ct to Leather Dr.

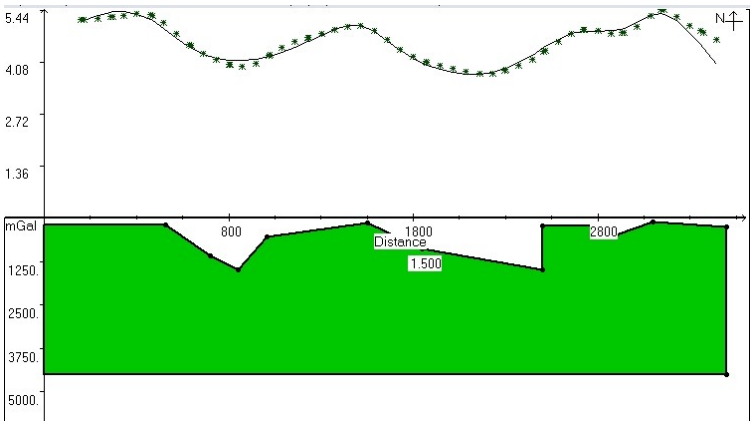

Figure 24 Profile FF', Green Horn View Ln to Cherokee Ln.

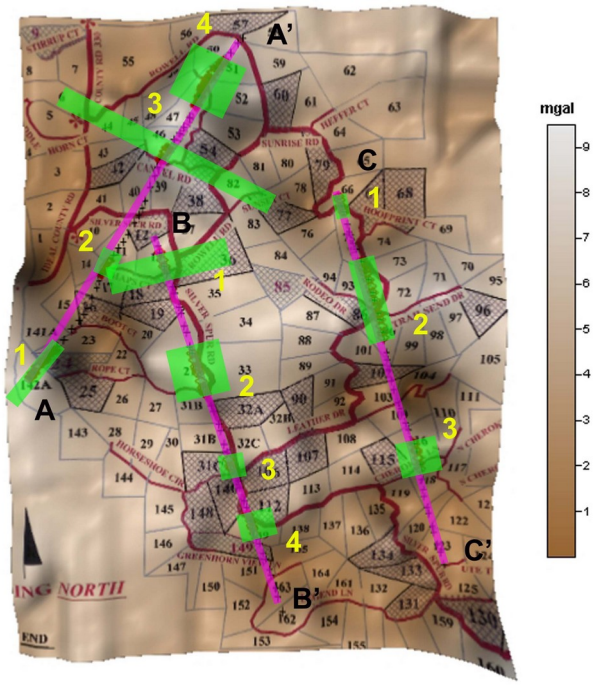

Figure 25 Lateral position of constant density gravity blocks marked in green.

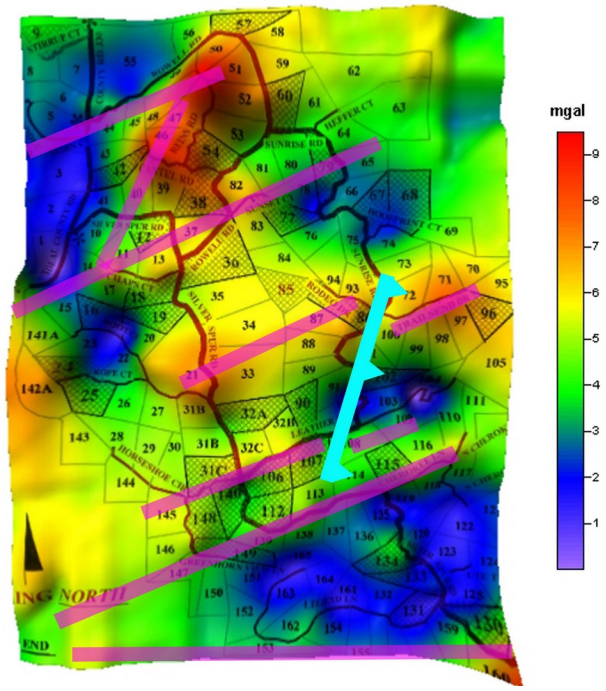

Figure 26 Final interpretation of dike locations. NNE trending fault in cyan is shown extending from Sunrise Rd to Leather Dr.

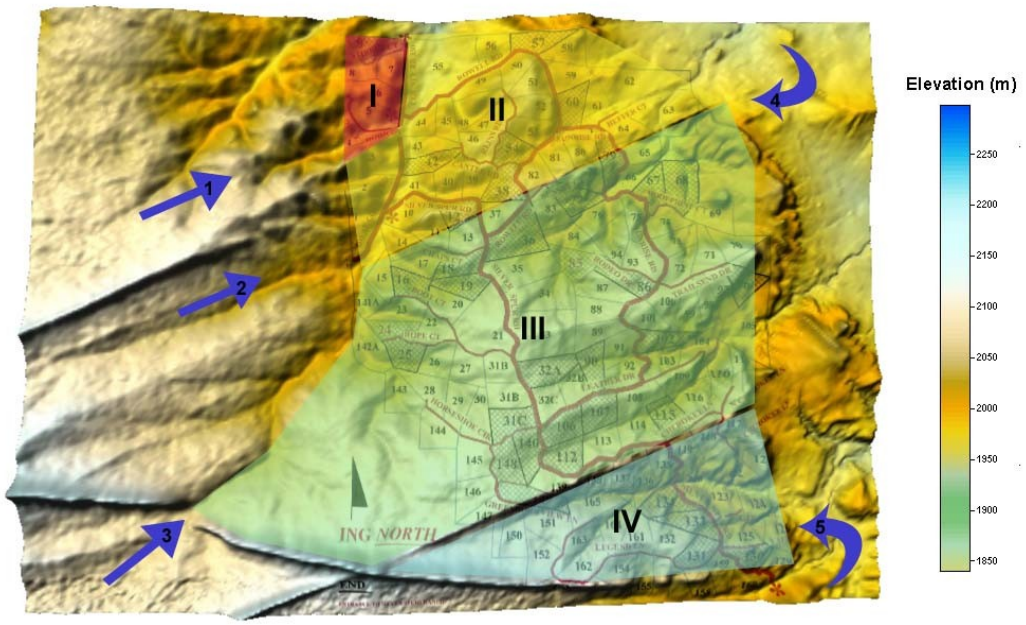

Figure 27 Water regions with recharge areas marked with blue arrows.

Appendix A

Gravity correction formulas

Drift correction:

$$g_{dc} = g_{obs} - [(g_{base2} - g_{base1})/(t_{base2} - t_{base1})]X(t_{obs} - t_{base1})$$

g_{obs} = observed gravity
g_{base} = gravity at base station
t_{obs} = time of gravity observation
t_{base} = time of observation at base station

Latitude correction:

$$g_{IGF} = 9.78032[(1 + 0.00193185138\sin^2 \lambda)/(1 - .006694379\sin^2 \lambda)^{1/2}]$$

λ = geographic latitude in radians

Free air correction:

g_{FA} = 0.3086*(surface elevation – datum elevation) elevation in meters

Bouguer correction:

$g_B = g_{FA}$ - 0.04193*density*(surface elevation – datum elevation)

for an average density of 2.67 g/cc

$g_B = g_{FA}$ - 0.112*(surface elevation – datum elevation)

g_B = 0.1966*(surface elevation – datum elevation) elevation in meters

Complete Bouger correction:

$g_{CB} = g_{dc} - g_{IGF} + g_B$ + terrain correction

Appendix B

Table 2 Gravity measurements and corrections.

Gravity units are in mgal. UTM XY locations and elevations are in meters.

stn	*x*	*y*	*elev*	*field g*	*rel g*	*latitude*	*free air*	*bouguer*	*complete*
B1	522518	4152400	2076	913.10	106.15	106.15	106.15	106.15	111.82
1	522501	4152445	2075	917.76	106.71	106.68	106.37	106.48	111.56
2	522603	4152467	2069	924.49	107.54	107.48	105.32	106.11	110.48
3	522703	4152480	2065	927.15	107.86	107.80	104.41	105.64	109.81
4	522806	4152490	2060	933.81	108.65	108.59	103.65	105.44	109.64
5	522905	4152503	2060	935.13	108.86	108.78	103.84	105.63	109.57
6	522998	4152533	2057	941.69	109.65	109.54	103.68	105.81	109.41
7	523092	4152572	2053	952.82	110.98	110.84	103.74	106.32	109.84
8	523186	4152602	2051	960.67	111.83	111.67	103.96	106.76	110.05
9	523280	4152639	2049	962.05	111.97	111.78	103.45	106.47	109.12
10	523373	4152678	2042	969.12	112.77	112.55	102.06	105.86	108.30
11	523457	4152730	2039	976.83	113.64	113.38	101.96	106.11	109.01
12	523546	4152775	2040	987.61	114.87	114.58	103.47	107.50	109.80
13	523639	4152816	2036	985.36	114.59	114.27	101.92	106.40	108.03
14	523720	4152875	2028	997.12	115.94	115.57	100.76	106.13	106.58
15	523786	4152916	2015	1005.54	116.90	116.49	97.67	104.50	104.78
16	523752	4152827	2013	1016.13	118.11	117.78	98.34	105.39	105.56
17	523832	4152855	2005	1038.55	120.69	120.34	98.43	106.38	106.74
18	523916	4152903	1999	1050.88	122.11	121.71	97.95	106.57	107.23
19	523976	4152989	1993	1062.21	123.40	122.94	97.33	106.62	107.25
20	524000	4153076	1992	1073.76	124.73	124.20	98.28	107.68	110.99
21	523056	4152638	2049	963.36	111.84	111.65	103.32	106.34	108.80
22	523078	4152738	2039	975.30	113.22	112.95	101.53	105.68	107.28
23	523150	4152801	2029	993.36	115.31	115.00	100.49	105.75	107.38
24	523097	4152873	2028	1005.85	116.75	116.38	101.57	106.94	107.70
25	523017	4152921	2017	1017.21	118.07	117.66	99.45	106.05	107.71
26	522990	4153015	2026	1008.03	116.98	116.49	101.06	106.66	109.52
27	523049	4153095	2034	1000.71	116.12	115.57	102.61	107.31	110.52
28	523089	4153173	2039	991.64	115.05	114.45	103.03	107.17	111.09
29	523007	4153234	2045	977.50	113.40	112.75	103.18	106.65	111.38
30	522920	4153281	2052	973.68	112.60	111.91	104.50	107.19	112.46
31	522847	4153346	2056	967.56	111.92	111.18	105.00	107.24	112.83
32	522829	4153424	2061	956.99	110.72	109.92	105.29	106.97	113.25
33	522884	4153514	2066	952.55	110.23	109.36	106.27	107.39	114.31
34	522970	4153557	2068	950.34	110.00	109.09	106.62	107.51	114.19
35	523062	4153598	2065	950.66	110.06	109.12	105.72	106.96	113.04
36	523151	4153650	2062	957.13	110.83	109.85	105.53	107.10	112.88
37	523230	4153772	2057	966.48	111.65	110.57	104.71	106.84	113.51
38	523146	4153831	2061	963.71	111.54	110.41	105.79	107.46	114.25
39	523063	4153894	2061	971.36	112.40	111.22	106.59	108.27	114.55
40	522975	4153931	2059	974.51	112.73	111.53	106.28	108.18	114.63
41	522871	4153945	2057	975.50	112.80	111.59	105.72	107.85	114.16
42	522782	4153982	2055	978.42	113.12	111.87	105.39	107.74	113.79
43	522688	4154074	2051	990.52	114.49	113.17	105.46	108.26	114.10
44	523330	4153737	2055	973.72	112.51	111.45	104.97	107.32	113.16
45	523429	4153732	2055	976.64	112.84	111.79	105.31	107.66	113.56

stn	x	y	elev	field g	rel g	latitude	free air	bouguer	complete
46	523524	4153766	2055	980.32	113.26	112.19	105.71	108.06	113.56
47	523605	4153821	2057	980.95	113.33	112.22	106.35	108.48	114.47
48	523693	4153870	2054	983.60	113.64	112.48	105.69	108.16	114.52
49	523788	4153892	2057	982.16	113.47	112.30	106.43	108.56	115.17
50	523883	4153920	2059	978.85	113.08	111.89	106.64	108.54	115.70
51	524007	4153978	2063	975.26	112.66	111.42	107.41	108.86	115.03
52	523285	4153856	2056	971.09	112.12	110.97	104.80	107.04	113.03
53	523325	4153950	2056	976.93	112.73	111.51	105.34	107.58	113.70
54	523325	4154050	2052	984.91	113.61	112.32	104.91	107.60	113.63
55	523254	4154124	2050	992.28	114.42	113.07	105.04	107.95	113.71
56	523190	4154207	2046	1001.95	115.49	114.06	104.81	108.16	112.89
57	523156	4154299	2038	1020.28	117.55	116.06	104.33	108.59	112.97
58	523119	4154391	2030	1039.73	119.75	118.19	103.99	109.14	112.56
59	523104	4154499	2019	1050.13	120.90	119.25	101.66	108.04	111.08
60	523149	4154578	2014	1057.98	121.76	120.04	100.91	107.85	110.29
61	523235	4154638	2007	1075.24	123.72	121.96	100.66	108.39	110.54
62	523293	4154714	2000	1090.13	125.40	123.58	100.13	108.64	110.42
63	523399	4154718	1999	1095.85	126.01	124.19	100.43	109.05	110.75
64	523485	4154674	1996	1095.44	125.91	124.12	99.43	108.39	109.63
65	523562	4154587	1995	1100.50	126.46	124.74	99.74	108.81	111.61
66	523123	4154685	2013	1067.29	122.50	120.71	101.26	108.32	111.48
67	523106	4154780	2012	1076.97	123.57	121.70	101.95	109.12	111.46
68	523021	4154837	2003	1097.94	125.95	124.03	101.50	109.67	111.41
69	522938	4154894	1996	1109.33	127.27	125.31	100.62	109.57	111.57
70	522847	4154873	1999	1110.72	127.43	125.48	101.72	110.34	112.18
71	522753	4154827	1998	1105.29	126.80	124.89	100.82	109.55	111.03
72	522666	4154838	1994	1105.29	126.80	124.88	99.57	108.75	110.16
73	522651	4154928	1992	1104.80	126.74	124.75	98.82	108.23	109.81
74	522724	4154999	1993	1107.83	127.34	125.29	99.68	108.97	110.63
75	522787	4155075	1990	1108.04	127.36	125.25	98.71	108.34	110.52
76	522819	4155167	1997	1110.58	127.65	125.47	101.09	109.93	112.37
77	522897	4155225	1996	1109.29	127.49	125.27	100.58	109.53	111.51
78	522891	4155317	1993	1115.88	128.25	125.95	100.34	109.63	111.29
80	522764	4155469	1991	1123.85	129.17	126.75	100.52	110.04	112.49
81	522721	4155563	1995	1123.65	129.14	126.65	101.65	110.72	112.68
79	522845	4155402	1992	1121.27	128.85	126.49	100.57	109.97	112.32
82	522659	4155638	1993	1128.18	129.65	127.10	101.48	110.78	112.88
83	522575	4155681	1990	1136.13	130.56	127.98	101.44	111.07	112.57
84	522616	4155758	1984	1147.90	131.92	129.28	100.89	111.19	112.59
85	522707	4155807	1981	1155.94	132.85	130.17	100.85	111.49	112.78
86	522803	4155866	1979	1161.76	133.52	130.79	100.86	111.72	113.64
87	522460	4155691	1988	1136.46	130.57	127.98	100.82	110.67	112.78
88	522360	4155686	1990	1132.73	130.13	127.54	101.00	110.63	112.82
89	522262	4155670	1991	1130.68	129.88	127.31	101.08	110.59	113.58
90	522131	4155670	1999	1117.25	128.31	125.74	101.97	110.59	113.81
91	522142	4155772	2000	1118.02	128.37	125.72	102.26	110.77	114.65
92	522123	4155874	2005	1115.08	128.02	125.29	103.38	111.32	115.85
93	522093	4155970	2010	1105.46	126.90	124.09	103.72	111.11	115.77
94	522066	4156055	2010	1100.80	126.35	123.47	103.10	110.49	114.96

stn	x	y	elev	field g	rel g	latitude	free air	bouguer	complete
95	522042	4156151	2007	1109.04	127.30	124.35	103.05	110.78	115.34
96	522016	4156250	2010	1100.68	126.32	123.29	102.92	110.31	115.32
97	521989	4156345	2010	1098.83	126.10	122.99	102.62	110.01	115.12
98	521927	4156433	2010	1100.97	126.34	123.17	102.80	110.19	115.60
99	521860	4156507	2012	1108.65	127.23	123.99	104.24	111.41	115.77
100	521775	4156561	2004	1114.43	127.89	124.62	102.40	110.46	114.26
101	521681	4156590	1999	1120.22	128.56	125.26	101.50	110.12	114.24
102	521588	4156573	1999	1129.98	129.69	126.40	102.64	111.26	114.68
103	521512	4156510	1993	1144.28	131.34	128.10	102.49	111.78	114.22
104	521420	4156456	1987	1151.66	132.19	129.00	101.53	111.49	113.72
105	521326	4156411	1981	1157.23	132.84	129.68	100.37	111.00	112.84
106	521235	4156376	1976	1158.92	133.04	129.91	99.05	110.25	111.45
107	521140	4156344	1972	1160.67	133.25	130.14	98.05	109.69	110.79
108	521045	4156309	1971	1166.16	133.89	130.81	98.41	110.16	110.98
109	520969	4156244	1971	1162.23	133.44	130.41	98.01	109.76	110.44
110	520884	4156187	1967	1178.76	135.37	132.38	98.75	110.95	111.14
111	520794	4156144	1959	1180.77	135.60	132.65	96.55	109.64	109.79
112	520692	4156136	1955	1182.74	135.84	132.89	95.55	109.10	109.23
113	520610	4156075	1957	1183.97	135.98	133.09	96.36	109.68	109.83
114	520535	4156010	1957	1189.74	136.66	133.81	97.09	110.41	110.85
115	520443	4155977	1950	1202.01	138.09	135.27	96.38	110.49	110.91
116	520360	4155923	1951	1191.48	136.87	134.09	95.51	109.51	109.62
117	520279	4155943	1960	1179.03	135.42	132.63	96.83	109.82	112.96
118	522037	4155555	1999	1109.63	127.40	124.92	101.16	109.78	112.64
119	521944	4155492	2000	1103.66	126.72	124.29	100.83	109.34	112.43
120	521862	4155429	2003	1099.33	126.23	123.84	101.31	109.49	112.77
121	521805	4155346	2009	1089.06	125.04	122.72	102.04	109.55	113.58
122	521739	4155268	2014	1073.88	123.29	121.03	101.90	108.84	113.65
123	521664	4155223	2022	1060.48	121.74	119.52	102.85	108.90	113.94
124	521541	4155238	2024	1065.32	122.31	120.08	104.03	109.85	115.68
125	521438	4155193	2032	1053.14	120.91	118.71	105.13	110.05	116.46
126	521351	4155221	2037	1042.76	119.71	117.49	105.46	109.82	116.66
127	521348	4155313	2040	1038.06	119.18	116.88	105.77	109.80	116.76
128	521364	4155409	2040	1030.20	118.27	115.90	104.79	108.82	115.81
129	521408	4155513	2039	1030.62	118.33	115.88	104.46	108.60	115.60
130	521462	4155604	2038	1031.67	118.46	115.94	104.21	108.46	115.48
131	521509	4155694	2037	1035.18	118.88	116.28	104.25	108.61	116.05
132	521574	4155770	2040	1035.60	118.93	116.28	105.17	109.20	116.99
133	521600	4155870	2042	1032.89	118.63	115.90	105.40	109.21	117.46
134	521569	4155966	2045	1036.47	119.06	116.25	106.68	110.15	118.42
135	521499	4156044	2044	1037.74	119.22	116.35	106.48	110.06	117.75
136	521443	4156129	2041	1045.04	120.07	117.13	106.33	110.25	117.20
137	521231	4155233	2042	1035.18	118.93	116.70	106.20	110.01	116.56
138	521144	4155285	2041	1037.79	119.23	116.96	106.16	110.08	117.15
139	521043	4155329	2042	1033.88	118.78	116.47	105.98	109.79	116.56
140	520993	4155429	2038	1043.28	119.88	117.49	105.76	110.02	116.47
141	520961	4155512	2034	1043.67	119.92	117.47	104.51	109.21	115.13
142	521618	4155101	2034	1031.88	118.56	116.43	103.47	108.17	115.02
143	521599	4155011	2044	1017.24	116.86	114.80	104.92	108.51	115.77

stn	x	y	elev	field g	rel g	latitude	free air	bouguer	complete
144	521666	4154931	2049	1008.66	115.86	113.87	105.53	108.56	115.62
145	521726	4154852	2048	1009.29	115.94	114.00	105.36	108.50	115.04
146	521743	4154795	2044	1010.90	116.12	114.24	104.36	107.95	114.02
147	521831	4154867	2042	1018.30	116.99	115.04	104.55	108.36	114.88
148	521916	4154934	2042	1018.49	117.01	115.01	104.52	108.33	114.93
149	522009	4154984	2042	1017.60	116.91	114.87	104.38	108.19	115.14
150	521678	4154719	2049	1008.91	115.90	114.07	105.74	108.76	115.29
151	521609	4154646	2046	1009.23	115.94	114.17	104.91	108.27	114.59
152	521536	4154576	2042	1009.95	116.03	114.31	103.82	107.62	113.47
153	521468	4154500	2042	1017.22	116.87	115.22	104.73	108.53	114.47
154	521392	4154433	2044	1010.84	116.13	114.53	104.65	108.24	113.91
155	521249	4154370	2046	1002.21	115.13	113.58	104.32	107.68	113.23
156	521209	4154473	2043	1021.91	117.38	115.74	105.56	109.25	114.48
157	521190	4154573	2035	1038.27	119.27	117.55	104.90	109.49	114.25
158	521182	4154678	2029	1044.54	119.98	118.19	103.68	108.94	113.36
159	521170	4154791	2024	1062.05	122.01	120.12	104.07	109.89	113.74
160	521077	4154830	2018	1071.43	123.08	121.17	103.27	109.76	113.09
161	520977	4154831	2013	1090.12	125.24	123.33	103.88	110.94	113.75
162	520874	4154822	2007	1095.90	125.90	123.99	102.70	110.42	112.44
163	520777	4154827	2000	1107.31	127.22	125.30	101.85	110.36	111.91
164	520663	4154829	1995	1116.02	128.21	126.30	101.30	110.37	111.53
165	520572	4154869	1990	1124.10	129.14	127.20	100.66	110.28	111.01
166	520482	4154913	1984	1134.21	130.30	128.32	99.93	110.23	110.38
167	520367	4154950	1973	1143.90	131.41	129.40	97.61	109.14	109.37
168	520272	4154891	1976	1146.40	131.68	129.72	98.86	110.05	110.18
169	520183	4154835	1972	1145.06	131.52	129.59	97.50	109.14	109.30
170	520027	4154750	1976	1138.61	130.75	128.89	98.03	109.23	109.37
171	520312	4156849	1950	1208.63	138.85	135.34	96.46	110.56	110.76
172	520314	4156744	1946	1211.01	139.12	135.70	95.58	110.13	110.27
173	520314	4156638	1949	1209.75	138.97	135.63	96.44	110.65	110.78
174	520312	4156538	1951	1199.17	137.74	134.47	95.90	109.89	110.03
175	520309	4156429	1952	1192.18	136.92	133.74	95.47	109.36	109.48
176	520306	4156333	1955	1185.16	136.10	133.00	95.66	109.20	109.38
177	520305	4156228	1957	1183.38	135.89	132.87	96.15	109.47	109.61
178	520298	4156128	1955	1184.38	136.00	133.06	95.72	109.27	109.42
179	520282	4156020	1959	1183.20	135.86	133.00	96.90	110.00	110.11
180	520262	4155917	1960	1178.09	135.26	132.49	96.69	109.68	109.83
181	520241	4155813	1958	1177.08	135.14	132.45	96.03	109.24	109.50
182	520230	4155712	1957	1175.63	134.97	132.36	95.63	108.95	109.22
183	520239	4155601	1958	1173.25	134.69	132.16	95.75	108.96	109.11
184	520249	4155506	1962	1163.70	133.57	131.12	95.94	108.71	108.87
185	520254	4155408	1963	1163.16	133.51	131.13	96.26	108.91	109.05
186	520254	4155307	1965	1160.50	133.19	130.90	96.65	109.07	109.22
187	520219	4155210	1966	1154.95	132.55	130.33	96.38	108.70	108.85
188	520189	4155116	1967	1147.46	131.67	129.53	95.89	108.09	108.23
189	520155	4155016	1973	1144.47	131.32	129.26	97.47	109.00	109.16
190	520099	4154927	1975	1140.92	130.91	128.92	97.75	109.05	109.28
191	520051	4154835	1976	1138.35	130.61	128.69	97.83	109.03	109.20
192	520010	4154729	1977	1134.24	130.14	128.30	97.75	108.83	109.22

stn	x	y	elev	field g	rel g	latitude	free air	bouguer	complete
193	519970	4154629	1983	1125.51	129.13	127.37	98.67	109.08	109.41
194	519915	4154542	1982	1117.42	128.19	126.50	97.49	108.01	108.18
195	519869	4154451	1981	1117.73	128.22	126.60	97.29	107.92	108.12
196	519837	4154344	1978	1113.25	127.71	126.17	95.93	106.90	107.03
197	519789	4154250	1984	1102.36	126.44	124.98	96.59	106.89	107.57
198	519680	4154181	1995	1087.42	124.71	123.30	98.30	107.37	108.30
199	519583	4154135	1999	1078.03	123.62	122.25	98.49	107.11	113.51
200	521263	4154274	2051	993.31	113.78	112.30	104.58	107.38	114.61
201	521165	4154236	2056	986.35	112.97	111.52	105.35	107.59	114.49
202	521068	4154192	2057	992.82	113.72	112.31	106.45	108.57	114.81
203	520970	4154186	2051	997.29	114.25	112.84	105.12	107.92	113.81
204	520868	4154221	2047	1002.26	114.83	113.39	104.44	107.69	113.36
205	520771	4154265	2041	1008.17	115.52	114.04	103.24	107.16	112.40
206	520672	4154278	2040	1013.04	116.09	114.61	103.50	107.53	112.37
207	520597	4154224	2037	1027.73	117.80	116.36	104.33	108.69	114.80
208	521255	4154168	2050	997.08	114.24	112.85	104.82	107.73	113.76
209	521228	4154068	2051	989.42	113.35	112.04	104.32	107.12	112.86
210	521213	4153968	2050	988.68	113.27	112.03	104.01	106.92	112.75
211	521315	4153902	2052	982.91	112.60	111.42	104.01	106.70	113.15
212	521370	4153815	2056	974.67	111.65	110.53	104.36	106.60	112.96
213	521426	4153732	2060	968.86	110.98	109.92	104.99	106.78	113.30
214	521475	4153644	2063	960.80	110.04	109.06	105.05	106.51	113.63
215	521502	4153548	2070	952.16	109.04	108.14	106.28	106.96	114.12
216	521509	4153446	2072	945.26	108.24	107.42	106.18	106.63	114.68
217	521493	4153341	2082	934.35	106.98	106.23	108.09	107.41	115.41
218	521529	4153252	2083	924.88	105.85	105.18	107.34	106.55	114.75
219	521603	4153180	2086	919.33	105.20	104.58	107.67	106.55	115.25
220	521624	4153075	2089	917.42	104.98	104.44	108.46	107.00	114.93
221	521574	4152945	2084	923.30	105.66	105.23	107.69	106.80	114.37
222	521474	4152980	2087	928.51	106.26	105.80	109.20	107.96	115.40
223	521366	4152996	2082	938.42	107.41	106.94	108.79	108.12	114.82
224	521267	4152959	2076	946.51	108.35	107.90	107.90	107.90	113.85
225	521164	4152953	2069	953.65	109.18	108.74	106.58	107.36	113.35
226	521057	4153029	2068	956.43	109.50	109.01	106.54	107.43	113.35
227	520962	4153114	2066	961.26	110.07	109.50	106.42	107.54	113.74
228	520934	4153221	2067	967.67	110.82	110.17	107.39	108.40	114.54
229	520901	4153309	2065	972.72	111.41	110.69	107.29	108.52	114.05
230	520845	4153400	2061	969.83	111.07	110.28	105.66	107.33	112.53
231	520738	4153437	2054	970.36	111.14	110.32	103.53	105.99	110.42
232	520662	4153472	2046	994.13	113.91	113.06	103.80	107.16	110.02
233	520611	4153584	2029	1013.64	116.18	115.24	100.74	106.00	108.35
234	520518	4153643	2023	1026.25	117.65	116.66	100.31	106.24	108.76
235	520423	4153687	2024	1029.52	118.03	117.01	100.96	106.79	109.87
236	520270	4153718	2029	1018.45	116.75	115.70	101.20	106.46	110.30
237	520152	4153681	2037	1005.35	115.23	114.21	102.18	106.54	110.52
238	520116	4153638	2039	996.25	114.17	113.19	101.77	105.91	111.35
239	520831	4153150	2061	961.18	110.10	109.51	104.88	106.56	111.63
240	520722	4153115	2058	970.32	111.17	110.61	105.05	107.07	111.48
241	520606	4153102	2055	974.95	111.71	111.15	104.67	107.03	110.98

stn	x	y	elev	field g	rel g	latitude	free air	bouguer	complete
243	520398	4153147	2047	981.36	112.46	111.86	102.91	106.16	110.60
242	520504	4153127	2052	984.55	112.83	112.25	104.84	107.53	111.34
244	520311	4153182	2045	988.71	113.31	112.69	103.12	106.59	110.34
245	520198	4153212	2044	999.79	114.60	113.96	104.08	107.66	110.64
246	520061	4153176	2037	1009.75	115.76	115.14	103.11	107.47	115.08
247	521608	4152825	2083	925.98	106.02	105.68	107.84	107.06	113.59
248	521660	4152733	2078	927.94	106.25	105.98	106.60	106.38	112.53
249	521709	4152635	2076	919.02	105.21	105.02	105.02	105.02	111.16
250	521771	4152517	2078	916.44	104.91	104.82	105.44	105.21	111.49
251	521803	4152422	2081	914.83	104.73	104.71	106.25	105.69	112.16
252	521845	4152304	2085	909.61	104.12	104.19	106.97	105.96	112.65
253	521876	4152201	2089	903.87	103.45	103.61	107.62	106.16	112.85
254	521887	4152145	2090	903.17	103.37	103.57	107.89	106.32	112.82
255	521782	4152102	2089	900.20	103.02	103.26	107.27	105.81	112.49
256	521658	4152087	2091	889.13	101.74	101.98	106.61	104.93	111.98
257	521575	4152059	2095	886.72	101.46	101.72	107.59	105.46	112.38
258	521473	4151998	2095	887.16	101.51	101.82	107.69	105.56	111.72
259	521360	4151955	2092	887.76	101.58	101.93	106.86	105.07	111.90
260	521381	4151844	2097	879.73	100.64	101.08	107.56	105.21	112.04
261	521357	4151739	2099	882.13	100.92	101.44	108.54	105.96	112.47
262	521378	4151639	2098	879.12	100.57	101.17	107.96	105.50	111.90
263	521413	4151506	2103	867.50	99.22	99.92	108.26	105.23	112.26
264	521461	4151373	2108	853.25	97.56	98.37	108.25	104.66	111.22
265	521594	4151327	2108	848.01	96.96	97.80	107.67	104.09	109.78
266	522403	4152396	2076	927.71	106.14	106.14	106.14	106.14	112.18
267	522312	4152355	2080	918.91	105.11	105.15	106.38	105.93	112.23
268	522215	4152327	2083	911.05	104.19	104.25	106.41	105.62	112.03
269	522131	4152268	2085	902.44	103.18	103.29	106.06	105.06	111.85
270	522035	4152197	2090	896.00	102.42	102.58	106.90	105.34	111.54
271	521957	4152134	2089	902.11	103.13	103.34	107.35	105.89	111.60
272	521902	4152025	2083	907.54	103.75	104.05	106.21	105.42	110.05
273	521921	4151923	2078	913.85	104.48	104.86	105.47	105.25	109.50
274	521908	4151831	2073	924.21	105.68	106.13	105.20	105.54	109.86
275	521933	4151711	2076	919.71	105.15	105.69	105.69	105.69	109.99
276	522041	4151654	2080	908.58	103.85	104.44	105.67	105.22	110.58
277	522152	4151593	2088	896.64	102.46	103.09	106.79	105.45	110.76
278	522265	4151567	2088	889.57	101.63	102.28	105.99	104.64	109.78
279	522353	4151625	2082	903.83	103.28	103.89	105.74	105.07	109.98
280	522456	4151684	2082	908.12	103.77	104.33	106.18	105.51	110.01
281	522527	4151738	2080	912.15	104.23	104.75	105.98	105.54	110.38
282	522634	4151753	2080	913.62	104.39	104.90	106.14	105.69	110.15
283	522727	4151767	2076	909.12	103.86	104.36	104.36	104.36	108.20
284	522805	4151826	2069	929.72	106.23	106.68	104.52	105.31	108.91
285	522896	4151869	2066	934.81	106.81	107.23	104.15	105.27	108.59
286	523001	4151893	2066	937.26	107.09	107.49	104.41	105.52	108.76
287	523101	4151891	2062	941.31	107.56	107.96	103.64	105.21	108.15
288	523198	4151901	2059	947.27	108.24	108.63	103.39	105.29	107.72
289	523298	4151894	2054	956.18	109.26	109.66	102.87	105.33	106.98
290	523371	4151833	2047	971.25	110.96	111.40	102.45	105.70	106.48

stn	x	y	elev	field g	rel g	latitude	free air	bouguer	complete
292	523468	4151685	2027	997.39	113.95	114.45	99.33	104.82	105.00
293	523495	4151604	2021	1011.88	115.63	116.19	99.22	105.37	105.87
294	523481	4151538	2017	1024.49	117.07	117.70	99.50	106.10	106.98
295	523460	4151388	1999	1046.83	119.66	120.34	96.58	105.20	107.99
296	523522	4151308	2013	1027.04	117.35	118.15	98.70	105.76	107.34
297	523573	4151229	2024	1015.39	115.98	116.84	100.79	106.61	107.39
298	523669	4151198	2030	999.00	114.06	114.98	100.79	105.94	106.35
299	523756	4151143	2032	982.25	112.10	113.05	99.47	104.40	104.66
300	523819	4151069	2033	981.21	111.96	112.95	99.68	104.50	104.89
301	523881	4150993	2033	984.63	112.36	113.41	100.14	104.95	105.42
302	523937	4150908	2028	993.68	113.40	114.51	99.70	105.08	105.82
303	523955	4150810	2037	974.15	111.13	112.31	100.27	104.64	105.09
304	523943	4150690	2041	956.62	109.09	110.34	99.54	103.46	103.81
305	523996	4150603	2039	966.16	110.20	111.54	100.13	104.27	104.69
306	524086	4150574	2036	974.84	111.20	112.62	100.28	104.75	105.39
307	524149	4150497	2031	984.95	112.37	113.82	99.93	104.97	106.33
308	524208	4150412	2024	991.71	113.16	114.66	98.61	104.43	106.58
309	524294	4150362	2015	1000.61	114.19	115.76	96.93	103.76	106.61
310	524396	4150348	2008	1018.43	116.26	117.86	96.88	104.49	108.41
311	524499	4150333	2004	1032.96	117.94	119.56	97.34	105.40	109.77
312	524590	4150298	1994	1044.88	119.33	120.96	95.65	104.83	110.32
313	524583	4150176	1986	1060.26	121.11	122.77	95.00	105.07	111.66
314	523407	4151952	2047	968.69	110.41	112.17	103.22	106.47	108.32
315	523489	4152009	2047	977.04	111.38	111.73	102.79	106.03	108.00
316	523564	4152078	2053	973.13	110.92	111.23	104.13	106.71	109.39
317	523644	4152143	2060	961.10	109.51	109.77	104.83	106.62	110.14
318	523726	4152200	2064	952.55	108.51	108.72	105.01	106.36	110.07
319	523828	4152204	2061	953.21	108.59	108.74	104.12	105.80	109.53
320	523932	4152225	2055	966.34	110.11	110.27	103.78	106.14	108.98
321	523954	4152323	2048	990.20	112.88	113.02	104.38	107.51	110.14
322	524016	4152427	2051	992.60	113.15	113.21	105.50	108.30	111.43
323	523919	4152118	2050	972.88	110.85	110.83	102.81	105.72	108.17
324	523900	4152019	2044	984.78	112.23	112.45	102.58	106.16	107.86
325	523960	4151936	2036	993.15	113.20	113.50	101.16	105.63	106.50
326	524011	4151855	2036	995.42	113.46	113.83	101.48	105.96	106.71
327	524100	4151789	2029	1003.51	114.39	114.82	100.32	105.58	105.79
328	524155	4151704	2018	1013.26	115.52	116.01	98.11	104.60	105.16
340	524053	4150698	2037	969.92	110.63	111.18	99.15	103.51	103.94
341	524156	4150691	2038	968.37	110.46	111.80	100.08	104.33	104.85
342	524255	4150693	2038	966.39	110.24	111.59	99.86	104.12	104.63
343	524358	4150701	2031	967.63	110.40	111.75	97.86	102.90	103.92
344	524457	4150732	2032	979.52	111.79	113.13	99.55	104.48	105.37
345	523784	4150520	2046	951.51	108.52	109.83	100.57	103.93	104.14
346	523691	4150471	2049	947.05	107.98	109.47	101.14	104.16	104.35
347	523595	4150473	2053	944.15	107.64	109.16	102.06	104.64	104.84
348	523489	4150480	2055	940.95	107.26	108.78	102.30	104.65	104.93
349	523379	4150568	2063	928.59	105.81	107.33	103.31	104.77	105.67
350	523300	4150631	2060	932.66	106.28	107.72	102.78	104.57	105.34
351	523194	4150640	2059	934.08	106.43	107.83	102.58	104.48	105.18

stn	x	y	elev	field g	rel g	latitude	free air	bouguer	complete
352	523042	4150676	2058	934.91	106.52	107.91	102.35	104.37	105.04
353	522953	4150678	2060	928.87	105.81	107.17	102.23	104.02	104.85
354	522832	4150676	2069	909.68	103.57	104.92	102.76	103.55	105.15
355	522680	4150677	2079	899.66	102.39	103.75	104.68	104.34	106.91
356	522607	4150618	2082	896.62	102.03	103.38	105.24	104.56	107.32
357	522546	4150522	2087	887.39	100.95	102.35	105.74	104.51	107.60
358	522454	4150459	2093	873.02	99.27	100.75	105.99	104.09	107.68
359	522329	4150430	2096	863.89	98.19	99.72	105.89	103.66	107.51
360	522223	4150436	2097	859.44	97.81	99.36	105.84	103.49	107.44
361	522122	4150461	2099	858.08	97.65	99.19	106.29	103.72	107.94
362	522043	4150522	2100	857.04	97.53	99.05	106.46	103.77	107.92
363	522088	4150678	2089	878.18	99.99	101.46	105.47	104.02	107.60
364	522164	4150752	2083	886.07	100.90	102.26	104.42	103.63	106.44
365	522183	4150854	2078	892.81	101.69	102.98	103.60	103.38	106.18
366	522236	4150937	2075	900.14	102.54	103.76	103.45	103.56	106.22
367	522320	4150991	2072	908.67	103.53	104.68	103.45	103.90	106.35
368	522417	4151032	2064	919.72	104.82	105.92	102.22	103.56	105.31

Appendix C

USGS Report FS-239-95

Introduction to Potential Fields: Gravity